Subcellular targeted anion transporters

William G. Ryder,[1,4,] Marcus E. Graziotto,[1] Aviva Levina,[1] Bryson A. Hawkins,[3] David E Hibbs,[3] Elizabeth J. New,[1,2,5] and Philip A. Gale.*[1,4,6]

[1] School of Chemistry, The University of Sydney, Sydney, NSW, 2006,

[2] Australian Research Council Centre of Excellence for Innovations in Peptide and Protein Science, The University of Sydney, Sydney, NSW, 2006, Australia.

[3] Sydney Pharmacy School, Faculty of Medicine and Health, The University of Sydney, NSW 2006, Australia.

[4] University of Technology Sydney, Faculty of Science, School of Mathematical and Physical Sciences, Ultimo, NSW 2007, Australia.

[5] Sydney Nano Institute, the University of Sydney, Sydney, NSW, 2006, Australia.

[6] Lead contact.

*Correspondence: philip.gale@uts.edu.au (P.A.G.)

SUMMARY

Synthetic anion transporters that mediate electroneutral (H^+/Cl^-) transport have demonstrated anti-cancer activity due to their ability to disrupt subcellular homeostatic environments. Elucidation of the cell death mechanism revealed the transporters' ability to neutralize lysosomal pH gradients and inhibit autophagy. However, their effect on other subcellular compartments is unknown. Herein, we disclose the first subcellular targeted anionophores that accumulate in various membrane bound organelles to bias their natural propensity to depolarize lysosomes. Confocal microscopy revealed the ability of the naphthalimide-based transporters to localize within their intended membrane-bound organelles. Analogues that contained endoplasmic reticulum (ER) and lysosomal targeting motifs showed an enhanced H^+/Cl^- transport ability and cytotoxicity compared to non-targeted analogues. Moreover, ER and mitochondrial localization was found to enhance apoptosis in cancerous cells. Our work provides an alternative approach to the design of therapeutically focused synthetic anion transporters and an insight into possible subcellular compartment-specific effects on homeostasis.

INTRODUCTION

The precise regulation of anionic species across phospholipid bilayers is fundamental to cellular signaling, pH regulation, osmotic balance, and many other biological processes crucial for cellular function.[1-3] Synthetic molecules capable of facilitating anion transmembrane transport have attracted significant interest as potential therapeutics, aiming to address diseases associated with ion dysregulation, such as cystic fibrosis, or to serve as novel anti-cancer agents.[4-6] Recently, synthetic anion transporters have been shown to match and even surpass the transport abilities of biological Cl^- channels and natural products.[7,8] As a result, there is a growing focus on evaluating their impact at a cellular level.[9] The current understanding is that anionophores can induce programed cell death, a process also known as apoptosis, by decreasing the lysosomal Cl^- concentration via electroneutral (H^+/Cl^-) transport. This perturbation of ion concentration leads to an increase in lysosomal pH and disruption of lysosomal function essential for autophagy.[10,11]

Mammalian cells are highly complex and possess many compartmentalized membrane-bound organelles, each with a specific structure and role vital for cellular function.

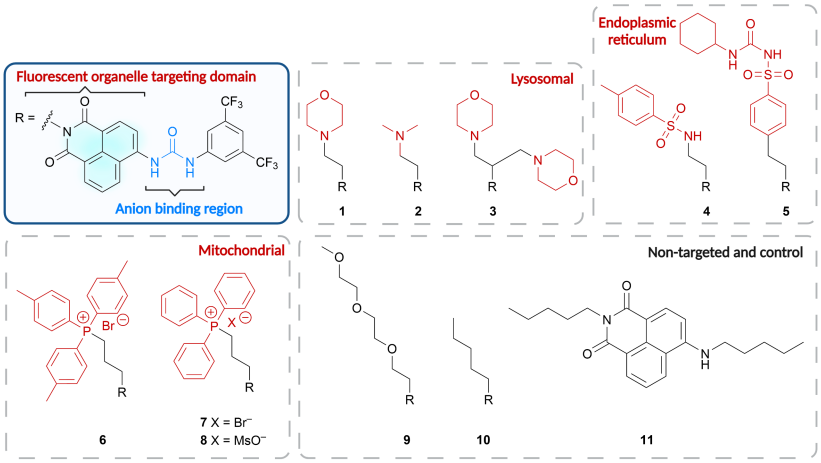

Figure 1 Structures of the fluorescent anion transporters studied in this paper.

Lysosomal targeting anionophores **1**–**3**, ER targeting anionophores **4** and **5**, mitochondrial targeting anionophores **6**–**8**, non-targeting anionophores **9** and **10**, and control naphthalimide **11**. Blue = anion binding motif. Red = subcellular targeting group.

Common examples include mitochondria, which form the foundation of energy production from oxidative phosphorylation.[12] The endoplasmic reticulum (ER) synthesizes lipids and proteins that are subsequently sorted and modified through post-translational modifications in the Golgi apparatus,[13,14] and lysosomes are responsible for cellular digestion essential to autophagy.[15] While previously-tested H^+/Cl^- transporting anionophores have been found to exert their cytotoxic effects through the lysosomes,[10] the effect of anionophore-induced transport on other subcellular compartments is currently unknown. Cl^- transport proteins have been identified in other subcellular compartments such as the ER, Golgi apparatus and mitochondria, which highlights the importance of this anion to the cellular function of many membrane-bound organelles.[16-19] We hypothesized that anionophores that can selectively target unexplored membrane-bound organelles might elicit different physiological responses.

Herein, we demonstrate this concept by developing a series of fluorescent anionophores, compounds **1**–**10** (**Figure 1**), that have been designed to localize in different subcellular compartments. The appendage of organelle-targeting motifs maintained, and in some cases increased, the anion binding and transport ability of the receptors, while live cell confocal laser scanning microscopy confirmed their intended organelle-specific localization. All the anionophores demonstrated cytotoxicity towards cancer cells. When compared to non-targeted analogues, transporters that demonstrated membrane-bound localization were found to enhance both their cytotoxicity and their ability to induce apoptosis towards cancerous cells. We believe that these findings offer an alternative approach in the advancement of synthetic anionophores and will aid in the future development of antineoplastic-oriented supramolecular agents.

RESULTS AND DISCUSSION

Compounds **1**–**11** (**Figure 1**) were constructed around a fluorescent 4-amino-1,8-naphthalimide core. The scaffold has been used extensively in sensing and cellular imaging due to its desirable photophysical properties.[20,21] Urea-based receptors have found numerous applications in the field of anion recognition due to their widely recognized binding properties and were chosen as the binding motif for compounds

1–**10**.[22] Moreover, we have previously demonstrated the anionophoric ability and cytotoxicity of compound **10**, which was found to disperse homogenously in the cytosol.[23] The 1,8-anhydride derivative of this scaffold allows for a high degree of functionalization which we chose to exploit through the appendage of subcellular targeting motifs. Additionally, the distal nature of the anhydride minimized possible sterically encumbering interactions between the targeting groups and the hydrogen bonding cavity.

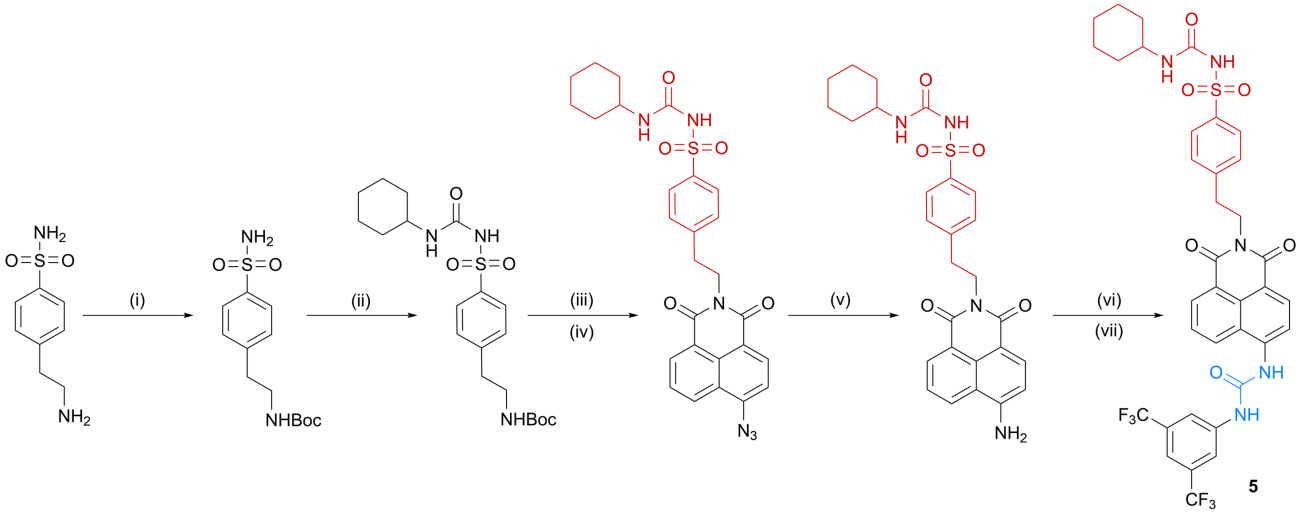

Scheme 1. Synthesis of ER-targeting anionophore 5

(i) Boc_2O, CH_2Cl_2, 96%.
(ii) Cyclohexyl isocyanate, acetone, K_2CO_3, 64%.
(iii) TFA, CH_2Cl_2.
(iv) EtOH, NEt_3, 4-azido naphthalic anhydride, reflux, 62% over two steps.
(v) Zn, NH_4Cl, H_2O, EtOH, reflux, 83%.
(vi) Triphosgene, NEt_3, CH_2Cl_2.
(vii) 3,5-Bis(trifluoromethyl)aniline, CH_2Cl_2, 30% over two steps.
Blue = anion binding motif. Red = subcellular targeting group.

Although numerous targeting motifs facilitate selective subcellular accumulation, many include highly charged moieties, hydrophilic scaffolds and peptide sequences, which are undesirable in the pursuit of efficient membrane permeation.[24] Therefore, we opted for the incorporation of simple lipophilic groups, which align well with the properties required for effective transmembrane transport. To target the lysosomes, we incorporated morpholino- and *N*,*N*-dimethylethyl motifs due to their reversible protonation at physiological pH.[25] Singular morpholino-containing probes have previously been shown to localize in the mitochondria as well as lysosomes.[26-28] Therefore, a simple bis-morpholino targeting motif was also prepared and installed onto the 1,8-naphthalimide core to further probe whether enhanced lysosomal localization could also be achieved compared to **1**, which contained a single morpholine unit. Cyclohexylsulfonylurea and *p*-toluenesulfonamide motifs were used for targeting the ER.[29-31] We utilized triphenyl phosphoniums to specifically target the mitochondria, as these moieties are renowned for their propensity to accumulate within the negatively charged inner mitochondrial membrane, facilitated by the transmembrane proton pump.[32,33] A non-targeting hydrophilic polyethylene glycol chain, compound **9**, was synthesized alongside the previously-studied compound **10** to probe the activity of the transporters in the absence of targeting groups.[23] Lastly, a non-targeting control bearing a secondary amine, compound **11**, was synthesized to evaluate the importance of the hydrogen bonding urea motif.

The synthesis of each anionophore **1**–**10** was achieved in 4–7 steps, each initiated by the construction of their respective targeting motif (**Scheme 1**). The appropriate ethyl- and propylamine precursors were then incorporated into the central scaffold in good to excellent yields through a condensation reaction with 4-bromo- or 4-azido-1,8-naphthalic anhydride. Subsequent substitution and azide reduction afforded the 4-amino intermediates, which were transformed into their respective isocyanates using triphosgene. The addition of 3,5-bistrifluoromethyl aniline afforded compounds **1**–**10** in poor to excellent yields. Compound **11** was ultimately synthesized from the condensation of amylamine with 4-bromo-1,8-naphthalic anhydride, followed by a substitution with a second equivalent of amylamine which afforded **11** in excellent and moderate yields, respectively. Complete details of synthetic procedures and characterization are provided in the supplementary information.

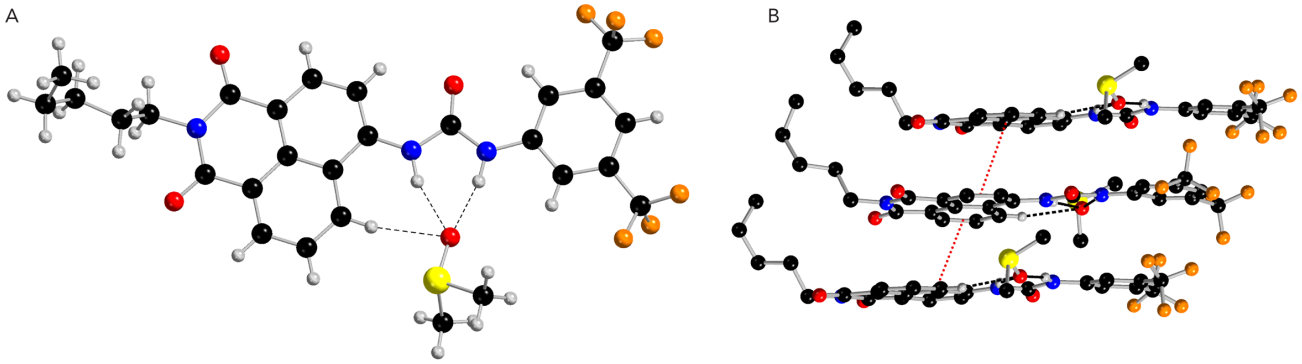

Figure 2. X-Ray crystal structure of 10.

(A) Crystal structure of **10** as a DMSO solvate, dashed lines indicate hydrogen bonds.
(B) Isolated trimer of **10** from the packing diagram viewed from the z-axis highlighting the aromatic cycle stacking interactions shown in red. All hydrogen atoms have been omitted for clarity, except for those directly involved in the hydrogen bonding interactions.

Single crystals suitable for X-ray diffraction were obtained through the slow evaporation of a concentrated solution of **10** in DMSO. Receptor **10** was crystalized as a 1:1 receptor:DMSO solvate (**Figure 2A**). As anticipated, the urea motif was found to form two NH hydrogen bonds to the sulfoxide (N–O′ distances 2.757–2.882 Å, N–H···O angles 160.8°–163.3°). Additionally, a weaker ancillary CH hydrogen bond was also formed from the C5 position on the naphthalimide scaffold, further encapsulating the bound DMSO within the binding cavity (C–O′ distance 3.387 Å, C–H···O angle 161.7°). In addition to the primary hydrogen bonding interactions, non-covalent aromatic cycle stacking was observed in the crystal structure of **10** between the adjacent aromatic naphthalimide cores (centroid–centroid distance of 3.6 Å), while the solvated urea moieties were orientated antiparallel to each other (**Figure 2B**).

Anion binding in solution

The binding affinities of compounds **1**–**11** were assessed using ^{1}H NMR titrations in DMSO-d_6/0.5% water. Solutions of each receptor were titrated with up to 200 equiv. of tetrabutylammonium chloride (TBACl). Large downfield shifts from both the urea NH resonances and smaller shifts from the aromatic naphthalimide CH resonance were observed upon the addition of TBACl for receptors **1**–**10**, indicative of anion complexation mediated by hydrogen bonding. While a separate downfield shift of the secondary amine resonance was exhibited by compound **11**. All receptors were fit to both 1:1 and 1:2 receptor:guest binding models using a global fitting applet to generate the association constants shown in **Table 1**.[34,35]

Table 1. Apparent association constants for compounds 1-11 with Cl^- (as its TBA salt) in DMSO-d_6/0.5% H_2O.

Compound	K_a [a]	K_{11} [b]	K_{12} [b]
1	163	-	-
2	171	-	-
3	153	-	-
4	191	-	-
5	-	260	7
6	156	-	-
7	269	-	-
8	299	-	-
9	165	-	-
10	177	-	-
11	2	-	-

Association constant (M^{-1}) calculated by fitting the change in chemical shifts upon addition of tetrabutylammonium chloride to a: [a] 1:1 binding model; [b] a 1:2 binding model. All errors <9%.

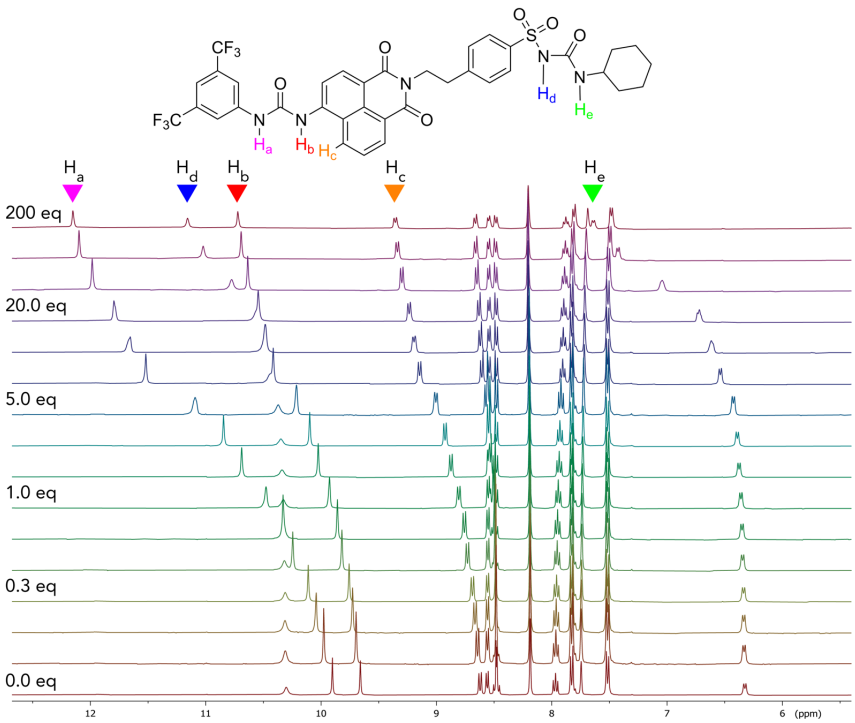

Figure 3. Stacked plot for the ^1H NMR titration (400 MHz) of 5 with TBACl in DMSO-d_6/0.5% H_2O.

Receptor **5** possesses a sulfonylurea on the appended targeting moiety, which has previously been used in the construction of anion receptors.[36] In the presence of Cl^-, downfield shifts were also observed by both sulfonylurea resonances of **5** (**Figure 3**) and accordingly, was the only receptor to exhibit a good fit to a 1:2 binding model whereas the remaining receptors displayed a better fit to a 1:1 binding model. Compounds **1**–**10** demonstrated moderate binding to Cl^-, while control receptor **11** showed almost no complexation to Cl^-, highlighting the importance of the dual hydrogen bonding motif for successful anion binding. The strongest affinity was

observed for receptors **7** and **8**, presumably due to additional electrostatic interactions from the charged targeting groups stabilizing the host-guest complex. The similarly charged receptor **6** showed the weakest complexation to Cl^-. While we anticipated a modest decrease in the positively charged character of the phosphonium ion in compound **6**, due to the positive inductive effects of the methylated aryl rings, the magnitude of this effect in the calculated association constants exceeded our expectations. The highest affinity across the neutral receptors was exhibited by receptor **4**. The single sulfonamide is likely too weak to create its own separate binding cavity but was found to enhance the overall affinity to Cl^-. Despite the incorporation of various targeting motifs, the binding affinities to Cl^- remained largely consistent across the neutral receptors, which justified our decision to position the targeting motifs away from the anion-binding motif.

Anion transport studies

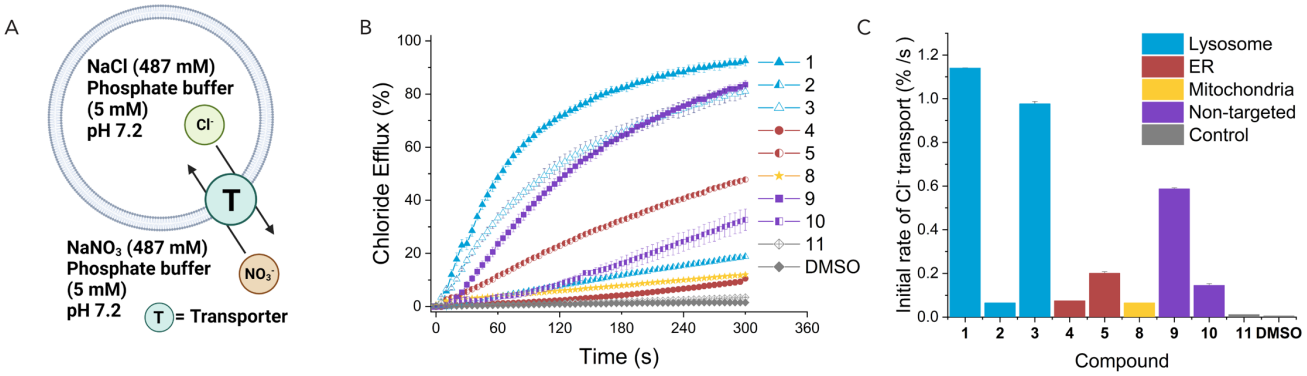

Figure 4. Determination of transport activity using the Cl^-/NO_3^- exchange assay

(A) Schematic of the Cl^-/NO_3^- exchange assay monitored by Cl^- ISE.
(B) Cl^- efflux as a function of time promoted by the addition of 1 mol% (with respect to lipid concentration) of compounds **1**–**5** and **8**–**11**.
(C) Calculated initial rates from the Cl^- efflux as a function of time promoted by the addition of 1 mol% (with respect to lipid concentration) of anionophores **1**–**5** and **8**–**11.**

Motivated by the binding capabilities of **1**–**10**, the anionophoric ability of the naphthalimides was demonstrated using the Cl^-/NO_3^- exchange assay.[37] Palmitoyl-2-oleoyl-*sn*-glycero-3-phosphocholine (POPC) large unilamellar vesicles (LUVs, 200 nm) were entrapped with NaCl (489 mM, buffered to pH 7.2 using phosphate salts) and suspended in an external solution of $NaNO_3$ (buffered under the same conditions). Transporters were added as a DMSO solution (10 μL) at t = 0 s to initiate anion exchange across the membrane, and the increase in extravesicular Cl^- concentration was measured using a Cl^- ion-selective electrode (ISE). The vesicles were treated with Triton X-100 at t = 300 s to lyse the contents into the external solution and calibrate the 100% Cl^- efflux value. **Figure 4** and **Table 2** show the results of the Cl^-/NO_3^- exchange experiments at 1 mol% loading of each anionophore (with respect to lipid concentration).

In comparison to the simple pentyl analogue **10**, the anionophores were all found to actively transport Cl^-, despite the added complexity of the affixed targeting moieties. It should be noted that the addition of compound **7** to the Cl^-/NO_3^- exchange assay led to a spike in the initial transport rate, presumably due to interference from the Br^- counter anion, and therefore was omitted from the assay. Additionally, the assessment of the anion transport ability of **6** could not be completed due to the insolubility of the receptor. Morpholine-appended compounds **1** and **3** displayed the highest potency across the series and were significantly more active than lysosomal-

targeting analogue **2**. Amongst the proposed ER targeting receptors, higher activity was exhibited by **5** compared to **4**, which could be rationalized by the presence of the additional anion binding motif within compound **5**. Membrane permeability is heavily inhibited by charged species and could be a possible reason for the lower transport activity demonstrated by the triphenyl phosphonium-containing compound **8**. Both compounds that lacked targeting groups, **9** and **10**, were shown to efficiently mediate Cl^-/NO_3^- exchange.

Table 2. Calculated initial rates ($k_{initial}$), EC_{50} values, Hill coefficients (n) and ClogP values for compounds 1–11 in the Cl^-/NO_3^-exchange assay.

Compound	Cl^-/NO_3^-exchange assay			ClogP [c]
	$k_{initial}$ [a]	EC_{50} [b]	n	
1	1.14	0.27	1.5	5.4
2	0.07	-	-	5.7
3	0.98	0.45	1.5	5.2
4	0.08	-	-	6.4
5	0.20	-	-	7.7
6	-	-	-	12.3
7	-	-	-	11.4
8	0.07	-	-	11.4
9	0.59	0.37	1.3	5.2
10	0.15	-	-	7.3
11	0.01	-	-	5.4

[a] Maximum initial rate (% s^{-1}) calculated at a loading of 1 mol%, by fitting efflux plot to a linear function. All errors <5%.

[b] EC_{50} at t = 270 s, reported in lipid to molar ratio (mol%).

[c] Average ClogP values calculated using Flare developed by Cresset Group.

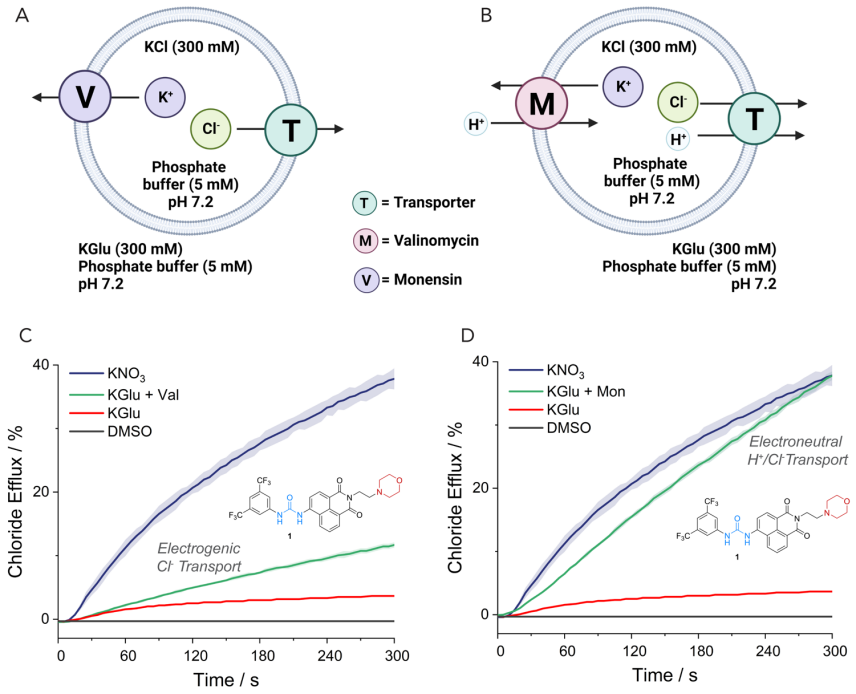

Figure 5 Determination of the Cl^- transport mechanism.

(A) Anionophore-facilitated electrogenic Cl^- transport. Coupling with valinomycin 'V' facilitated electrogenic K^+ transport, leading to net KCl efflux.
(B) Anionophore-facilitated H^+/Cl^- symport (or Cl^-/OH^- antiport shown in brackets). Coupling with monensin 'M' facilitated K^+/H^+ antiport, leading to net KCl efflux.
Comparison of the electroneutral and electrogenic transport of **1** in the presence of (C) valinomycin and (D) monensin.

Remarkably, the addition of the polyethylene glycol chain to compound **9** resulted in a four-fold increase in the Cl^-/NO_3^- exchange rate compared to the highly lipophilic pentyl analogue **9**. Moreover, receptor **9** was shown to be one of the most active anionophores that bears the highly hydrophilic group and has the potential to enhance the intrinsic deliverability of anionophores in aqueous solutions while retaining potent activity, an active area of transmembrane transport supramolecular chemists are persistently looking to explore.[38-42]

Overall, the transport activity was found to contest the trends uncovered in the solution-phase binding studies. This is a consequence of the targeting groups influencing the ability of each anionophore to partition through the membrane. Lipophilicity determines the ability of a transporter to partition through the lipid bilayer and has been demonstrated to be an important consideration when determining transmembrane transport activity. While no conclusive correlation was elucidated with respect to their ClogP values (**Table 2**), we found that the structurally simple targeting groups displayed the highest rate of Cl^-/NO_3^- exchange. From this, we theorized that the diminished activity observed could result from possible adverse interactions with the phospholipid bilayer from transporters that possess an inherent charge or additional hydrogen bond donors.

We then sought to determine the mechanism of Cl^- transport mediated by the anionophores using a cationophore-coupled assay using natural ionophores, valinomycin and monensin (**Figure 5**). POPC LUVs loaded with KCl (300 mM, buffered to pH 7.2 using phosphate salts) were suspended in potassium gluconate (KGlu, 300 mM, buffered to pH 7.2 using similar conditions). Transporters were added as a

DMSO solution (10 μL) at t = 0 s to initiate efflux, and the increase in Cl^- concentrations in the external solution was measured using an ISE. The vesicles were treated with Triton X-100 at t = 300 s to lyse all contents into the external solution and calibrate the 100% Cl^- efflux value.

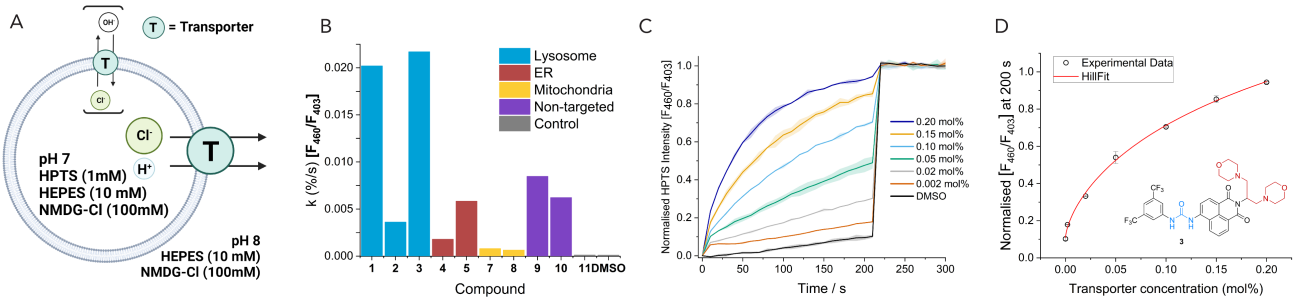

Figure 6 Determination of H^+/Cl^- transport activity using a fluorescence-based assay.

(A) Schematic of the HPTS assay monitored through the change in the fluorescence emission spectra of HPTS.
(B) H^+/Cl^- efflux as a function of time promoted by the addition of 0.2 mol% (with respect to lipid concentration) of compounds **1**–**5** and **7**–**11**.
(C) Dose response anion transport activity of **3**.
(D) Hill analysis of the H^+/Cl^- transport facilitated by **3**.

Electrogenic transport implies the transmembrane uniport of Cl^-, which generates a membrane potential that can be balanced through an independent electrogenic transport event (for example, the transport of a cation or back exchange of another anion). In contrast, electroneutral transport does not lead to a net transfer of charge. Instead, it involves the simultaneous transport of two ions (one anion and one cation, or two different anions) in a process which cannot be separated. The external solution utilizes the highly hydrophilic and membrane-impermeable gluconate; thus, the addition of the anionophore alone will not initiate transport as there is no counterflow of anions to alleviate the build-up of negative charge. Valinomycin strictly mediates the uniport of K^+ across the phospholipid bilayer and, consequently, coupling to valinomycin signifies the electrogenic uniport of Cl^- facilitated by the anionophore (**Figure 5A**). In contrast, monensin exchanges H^+/K^+ across the lipid membrane and coupling of an anionophore to monensin implies an electroneutral H^+/Cl^- symport mechanism mediated by the transporter (**Figure 5B**). A separate run using KNO_3 as an external solution was also performed as a control, to ensure the activity of the transporters aligned with the previous Cl^-/NO_3^- exchange assay. We concluded that anionophores **1**–**5** and **8**–**10** were capable of both electrogenic and electroneutral Cl^- transport, with a modest selectivity for H^+/Cl^- transport across all the tested anionophores (**Figure 5C** and **Figure 5D**). Implementing different targeting motifs offered no overall change in the transport mechanism, even in the presence of additional binding components, in the form of sulfonylureas, or electrostatic charges.

The H^+/Cl^- transport activity was further evaluated through a fluorescence-based assay (**Figure 6A**).[43] POPC LUVs were loaded with the pH-responsive fluorophore 8-hydroxypyrene-1,3,6-trisulfonate (HPTS) and N-methyl-D-glucamine (NMDG) chloride, buffered to pH 7.0 with HEPES. The vesicular solution was suspended in an external aqueous solution of NMDG-Cl, similarly, buffered to pH 7.0 with HEPES. A pH gradient was applied across the membrane through the addition of an NMDG base pulse, followed by the addition of the transporter as a DMSO solution (5 μL) to initiate transport. The ability of a transporter to dissipate the pH gradient through H^+/Cl^- symport (or equivalent OH^-/Cl^- antiport) was determined through the change in the fluorescence emission spectra of HPTS. At the end of the run, the vesicles were similarly treated with Triton X-100 to calibrate the 100% Cl^- efflux value. **Figure 6** and

Table 3 show the results of a HPTS-based experiment at 0.2 mol% loading of each anionophore (with respect to lipid concentration), alongside the dose-responsive behavior and Hill analysis of transporter **3**.

The assay allowed the comparison of the two mitochondrial targeting compounds **7** and **8**, whereby a marginal increase in the transport rate was observed upon the substitution of the Br^- counterion for MsO^-. To further quantify the anionophoric ability, the same assay was used to determine the concentration-dependent transport activity of each receptor. Dose-response curves were fit to the Hill equation to derive the effective concentration of a transporter required to reach 50% efflux (EC_{50}). An activity sequence of **3** > **1** > **9** > **2** = **5** > **10** was established, highlighting the high potency of the morpholine-appended anionophores **3** and **1**, with calculated EC_{50} values of 0.06 and 0.07 mol%, respectively (**Table 3**).

Table 3. Calculated initial rates ($k_{initial}$), EC_{50} values and Hill coefficients (n) for compounds 1–11 in the Cl^-/NO_3^- exchange assay. IC_{50} values of compounds 1–11 on the human lung carcinoma (A549) cell line after incubation for 24 h.

Compound	HPTS fluorescence-based assay			Cell viability
	$k_{initial}$[a]	EC_{50}[b]	n	IC_{50}[c]
1	20.2	0.07	1.1	4.4
2	3.6	0.14	1.8	5.3
3	21.7	0.06	0.7	3.3
4	1.8	-	-	35.1
5	5.8	0.14	0.7	6.6
6	-	-	-	-
7	0.6	-	-	11.9
8	0.8	-	-	11.4
9	8.5	0.09	1.3	>100
10	6.2	0.23	1.1	12.0
11	0.1	-	-	>200

[a] Maximum initial rate (% $\times 10^{-3} s^{-1}$) calculated at a loading of 0.2 mol%, by fitting the efflux plot to a linear or exponential decay function. All errors <10%.

[b] Effective concentration needed to obtain 50% Cl^- efflux (EC_{50}) at 210 s, values reported in transporter to lipid molar ratio (mol%).

[c] Half maximum inhibitory concentration (IC_{50}, μM) values of compounds **1–11** on the human lung carcinoma (A549) cell line after incubation for 24 h.

Alkyl chains are commonly employed in transmembrane transport to enhance lipophilicity and increase the membrane permeability of transporters.[44,45] A comparison of the EC_{50} values revealed that the substitution of the pentyl chain with various subcellular targeting motifs caused a small deviation in their anionophoric ability, with an enhanced activity observed for some of the anionophores. The most significant example was found in comparison of compounds **1** and **3**, where a four-fold decrease in the EC_{50} was observed. The Cl^- efflux mediated by **4** was found to plateau at 48%, even at high doses of the transporter, and thus Hill analysis could not be accurately carried out. Additionally, the triphenyl phosphonium-appended anionophores **7** and **8** showed little activity. This may be attributed to the cationic nature of the targeting motif which hinders the translocation of the free receptor across the phospholipid bilayer. The cationic charge on the phosphonium ion in compounds **6–8** is delocalized over three conjugated aryl rings to enhance mitochondrial membrane permeability. While this might counteract the negative effect of the cationic charge on transmembrane transport, the significant increase in lipophilicity may cause the transporters to embed themselves within the lipid membrane, reducing its access to the Cl^- in the aqueous bulk, leading to the poor activity observed in both assays.

The calculated Hill coefficients agreed with results from the Cl^-/NO_3^- exchange assay which confirmed a 1:1 transporter-anion stoichiometry. It was therefore concluded that the introduction of various targeting moieties bared no effect on the stoichiometric transport process of the series.

Subcellular localization

After establishing the anionophoric activity of the series, attention turned to exploring the subcellular localization of **1**–**11** in cultured cells. To confirm that the compounds were suitable for cellular imaging, the cell viability at concentrations of transporters intended for imaging studies was assessed using an alamarBlue assay in A549 human lung carcinoma cells (see supporting information). Most transporters displayed negligible cytotoxicity to the living cells when dosed with 1.5 μM for 24 h. Anionophore **3** showed modest toxicity, but due to the short incubation period for the localization experiments, it was deemed sufficient to proceed.

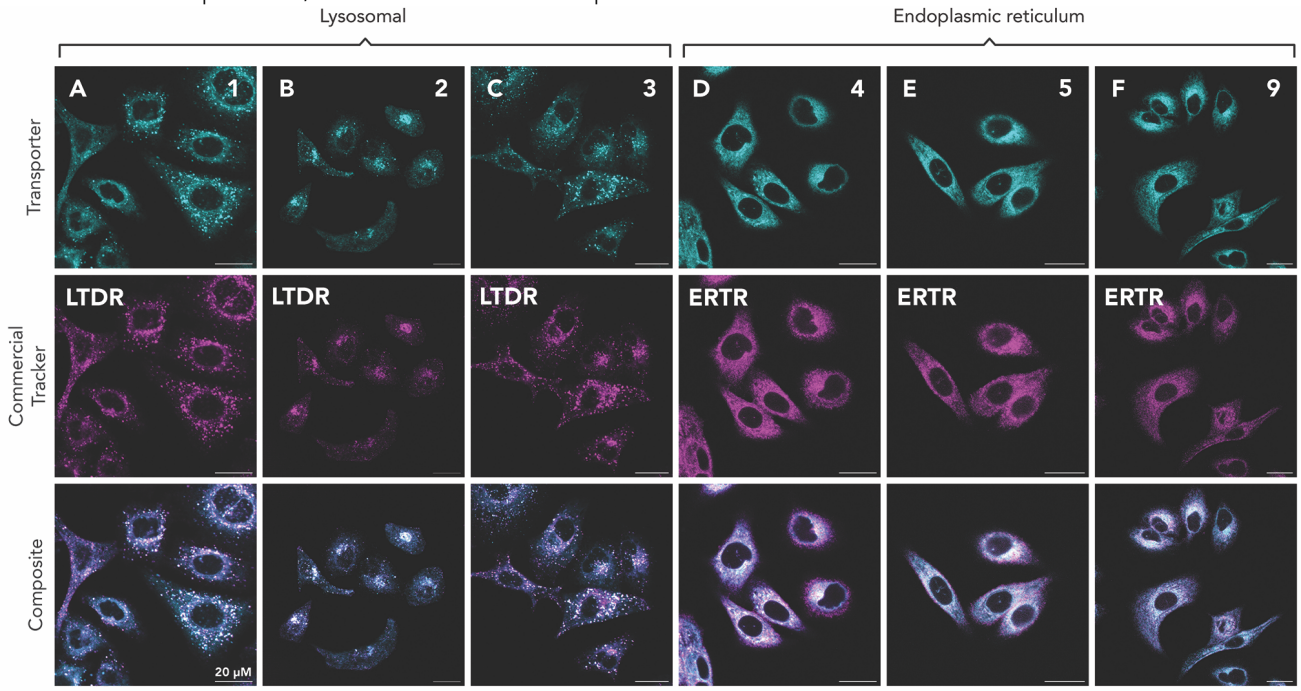

Figure 7 Colocalization experiments.

Representative images of live A549 cells dosed with:
LysoTracker Deep Red (LTDR) (50 nM) and 1 μM of transporter **1** (A), **2** (B), and **3** (C) for 30 mins. Cyan channel (transporters): λ_{ex} = 405 nm, λ_{em} = 410–510 nm. Magenta channel (LTDR): λ_{ex} = 640 nm, λ_{em} = 650–750 nm.
ER-Tracker Red (ERTR) (50 nM) and 1 μM of transporter **4** (D), **5** (E), and **9** (F) for 30 mins. Cyan channel (transporters): λ_{ex} = 405 nm, λ_{em} = 410–510 nm. Magenta channel (ERTR): λ_{ex} = 561 nm, λ_{em} = 575–675 nm.
All scale bars represent 20 μm.

Initial live cell imaging was performed with A549 cells, separately dosed with **1** at a concentration of 5 μM, 2.5 μM or 1 μM, and incubated for 30 min. Bright intracellular fluorescence was demonstrated across all concentrations when excited with a 405 nm laser (see supplemental information). To ensure the localization of the transporters was not masked at high concentrations, experiments were performed at a transporter concentration of 1 μM.

All subcellular targeting anionophores were found to localize in their intended subcellular compartments (**Figure 7** and **Figure 8**). The emissions of the lysosomal targeting transporters are shown in **Figure 7**, where punctate structures around the

nucleus indicative of lysosomal staining were observed. To confirm the accumulation of **1**–**3** within the desired organelle, colocalization experiments were performed with LysoTracker Deep Red (LTDR) (**Figure 7A**–**C**). The superposition of fluorescence images of the transporters and the lysosomal stain initially confirmed the lysosomal targeting ability of **1**–**3**. Pearson's correlation coefficients (PCC) values were obtained to quantify the co-localization and were calculated to be 0.80, 0.80 and 0.84 for transporters **1**, **2**, and **3**, respectively, which confirmed their affinity to localize in the lysosomes. The PCC values also highlighted that the presence of an additional morpholine motif in transporter **3** further enhanced its lysosomal accumulation when compared to **1**, which contained a single morpholine unit. This bis-morpholino motif, which can be readily synthesized and incorporated into target molecules, is a promising lysosomal targeting strategy that we are continuing to study in more detail.

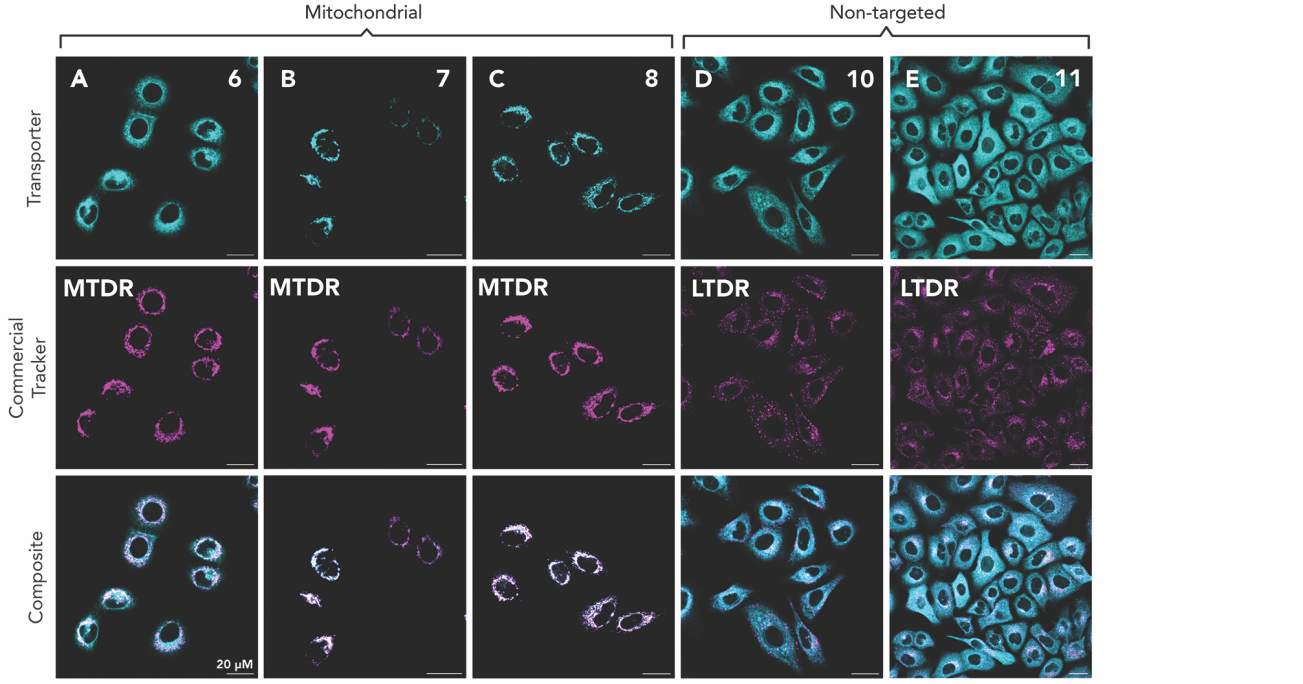

Figure 8 Colocalization experiments.

Representative images of live A549 cells dosed with:
MitoTracker Deep Red (MTDR) (50 nM) and 1 μM of transporter **6** (A), **7** (B), and **8** (C) for 30 mins Cyan channel (transporters): λ_{ex} = 405 nm, λ_{em} = 410-510 nm. Magenta channel (MTDR): λ_{ex} = 640 nm, λ_{em} = 650–750 nm.
LysoTracker Deep Red (LTDR) (50 nM) and 1 μM of transporter **10** (D) for 30 mins. Cyan channel (transporters): λ_{ex} = 405 nm, λ_{em} = 410-510 nm. Magenta channel (LTDR): λ_{ex} = 640 nm, λ_{em} = 650–750 nm.
LysoTracker Deep Red (LTDR) (50 nM) and 1 μM of transporter **11** (E) for 30 mins. Cyan channel (transporters): λ_{ex} = 405 nm, λ_{em} = 482-582 nm. Magenta channel (LTDR): λ_{ex} = 640 nm, λ_{em} = 650–750 nm.
All scale bars represent 20 μm.

Similar co-staining experiments with ER-Tracker Red (ERTR) determined that compounds **4** and **5** localized within the ER, with calculated PCC values of 0.78 and 0.74 (**Figure 7D**–**E**). Fluorescence images containing transporters **7** and **8** showed web-like fluorescent structures that correlated to the mitochondria (**Figure 8A**–**C**). The excellent mitochondrial targeting capabilities of compounds **7** and **8** were confirmed through their colocalization with MitoTracker Deep Red (MTDR), which gave calculated PCC values of 0.92 and 0.91, respectively. The almost identical PCC values established that the change in counter anion does not perturb the subcellular targeting ability of the transporters. Interestingly, the methylated triphenyl phosphonium motif showed less marked mitochondrial localization (**Figure 8A**).

Non-targeting compound **10** and control compound **11** were observed to localize homogenously throughout the cytoplasm, with no observable colocalization with any organelle marker (see supplementary information and **Figure 8D–E**). It was envisaged that incorporating a polyethylene glycol chain would promote cytosomal accumulation due to the high hydrophilicity of this motif. No lysosomal or mitochondrial accumulation was observed for transporter **9** (see supplementary information). However, modest localization (PCC = 0.65) in the ER was observed (**Figure 7F**). While lipophilic compounds tend to localize in the ER, the mechanistic reasoning is poorly understood compared to other organelles. Localization to the ER by non-targeting probes is believed to be a direct result of a molecule's optimum hydrophobicity towards the organelle and was hypothesized as the reason for the unexpected localization of transporter **9**.[46]

Cell viability

The cellular effects of compounds **1–5** and **7–11** were further investigated by exploring their cytotoxicity in more detail using an alamarBlue assay. The assessment of cell viability using compound **6** could not be completed due it's insolubility at the required concentrations in aqueous solution. Through the calculated half maximum inhibitory concentration (IC_{50}) values, it was found that all urea-containing transporters induced cell death after 24 h, albeit to varying degrees (**Table 3**). Compound **11** was non-toxic, highlighting that the observed cytotoxicity in the cancer cell line is strongly correlated to the presence of the anion binding urea moiety.

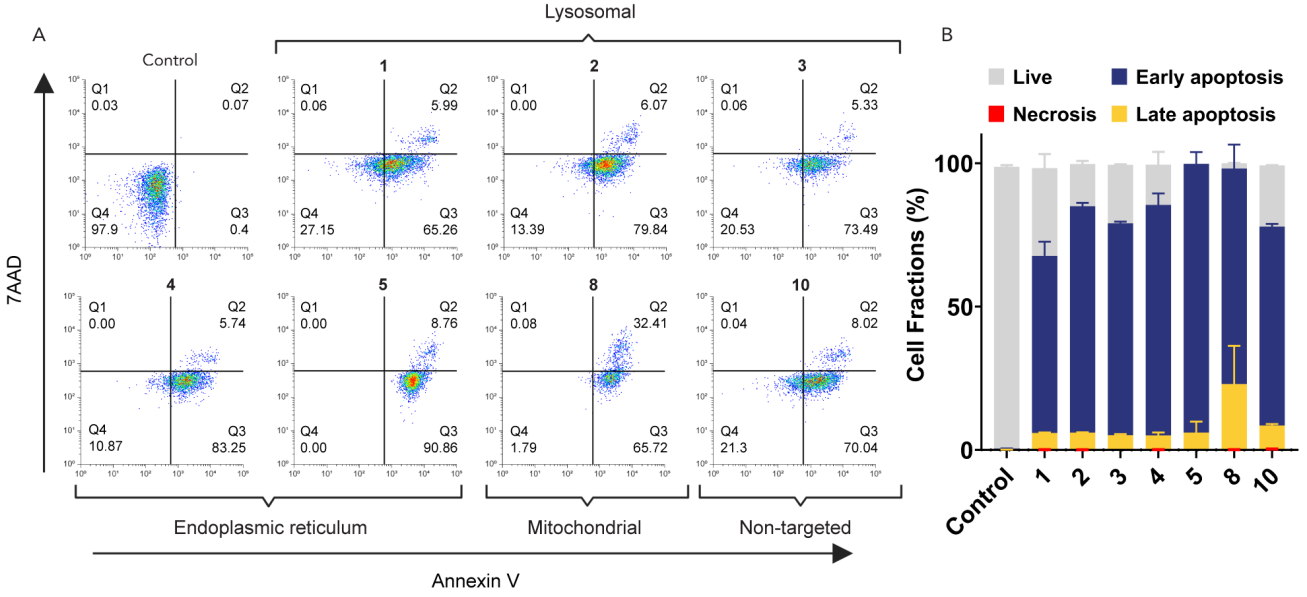

Figure 9. Determination of the cell death mechanism.

(A) Representative fluorescence-activated cell sorting of 7-AAD and FITC Annexin V stained A549 cells treated with **1–5**, **8** and **10** at their IC_{50} concentrations for 24 h, with the associated percentages shown for each quadrant. Live cells were defined as Annexin $V^-/7\text{-}AAD^-$ (Q4), early apoptosis as Annexin $V^+/7\text{-}AAD^-$(Q3), late apoptosis as Annexin $V^+/7\text{-}AAD^+$ (Q2), and necrosis as Annexin $V^-/7\text{-}AAD^+$ (Q1).
(B) Percentage of live cells (Annexin $V^-/7\text{-}AAD^-$; grey), early apoptotic cells (Annexin $V^+/7\text{-}AAD^-$; blue), late apoptotic (Annexin $V^+/7\text{-}AAD^+$; yellow) and necrotic cells (Annexin $V^-/7\text{-}AAD^+$; red) after treatment with **1–5**, **8** and **10** for 24 h. Bars represent the average of the experiment, error bars represent the standard deviation.

The extent of cytotoxicity from the lysosomal, ER, and mitochondrial targeted compounds was maintained despite their distribution to other subcellular components. The cell viability values for mitochondrial targeting transporters **7** and **8** were similar to non-targeting anionophore **10** (IC_{50} = 11.9 μM, 11.4 μM, and 12.0 μM,

respectively). Further comparison revealed no significant difference between compounds **7** and **8**, further highlighting the small effect of the change in counter ion. The more potent anionophores within the lysosomal and ER targeting groups demonstrated the highest cytotoxicity after 24 h. Lysosomal targeting anionophores **1**–**3** exhibited significant cytotoxicity towards the cell line (IC_{50} < 5 μM) and demonstrated the largest enhancement in cell death when compared to the non-targeting anionophore **10**. While the cell death mechanism of **10** is yet to be elucidated, it is possible that the lysosomal depolarization pathway shown by other anionophoric scaffolds is responsible for the observed cytotoxicity for transporters **1**–**3**.[10,11,47] It was postulated that the increase in lysosomal accumulation demonstrated by **1**–**3** over **10**, led to an increased perturbation of the lysosomal ionic and pH gradients, consequently enhancing the cytotoxicity. The sulfonylurea containing receptor **5** demonstrated potent toxicity and was significantly more toxic than compound **4** (IC_{50} = 6.6 μM and 35.1 μM, respectively). Additionally, the subcellular ER accumulation of compound **5** led to a two-fold increase in its antineoplastic activity when compared to non-targeting anionophore **10**.

It is well established that anionophores can induce cell death through apoptosis.[10,11,45,48,49] Flow cytometric analysis of double stained cells with FITC Annexin V and 7-AAD was performed to confirm the cell death mechanism of the anionophores (**Figure 9**). During apoptotic cell death, phosphatidylserine is exposed on the outer leaflet of the plasma membrane. Annexin V has a high affinity to phosphatidylserine, and thus its conjugation to the fluorochrome FITC allows for the flow cytometric analysis of cells undergoing apoptosis. 7-AAD is a cell impermeable DNA intercalator, which is only able to bind/intercalate to DNA upon loss of membrane integrity and was added to distinguish late apoptotic or necrotic cells.[50]

A549 cells were incubated with cytotoxic transporters **1**–**5**, **8** and **10** at their IC_{50} concentrations for 24 h, before labelling with the fluorescent markers. Compared to the untreated control, a significant increase in early- and late-stage apoptosis was observed by all tested anionophores (**Figure 9B**), highlighting the ability of the subcellular targeted library to induce cancer cell death through apoptosis. The highest percentage of apoptotic cells were not observed by the most cytotoxic compounds as determined by the alamarBlue IC_{50} assay. Instead, the ER and mitochondrial targeted transporters **4**, **5**, and **8** were found to induce the highest percentage of apoptotic cells. Notably, ER targeting compound **5** showed all analyzed cells to be in either early- or late-stage apoptosis. Demonstrated molecular mechanisms have previously correlated the induction of apoptosis to ER and mitochondrial stress through the disruption of homeostatic environments.[51-55] It is possible that the organelle localized perturbation of ionic and pH gradients through H^+/Cl^- transport in these two microenvironments may have led to the observed increase in apoptotic cells. We are continuing to investigate how these anionophores cause ER or mitochondrial stress.

Conclusion

We have presented here the first examples of subcellular targeted anionophores which accumulate in organelles previously unexplored within anion transmembrane transport. The addition of organelle-specific motifs to a naphthalimide scaffold afforded a library of fluorescent receptors capable of anion binding and transmembrane transport at micromolar concentrations. By exploiting lipophilic subcellular targeting motifs, we enhanced the electroneutral Cl^- transport ability of the anionophores compared to their non-targeted analogues. Fluorescence microscopy in live cells confirmed concentrated anionophoric accumulation in their intended membrane-bound organelles. Subcellular distribution of the transporters was shown to enhance the cytotoxicity towards a cancerous cell line. Moreover,

localization within the ER and mitochondria was shown to increase the transporters' ability to induce apoptosis. We anticipate that the cellular manipulation of anionophores will open novel possibilities for initiating new subcellular compartment-specific effects on homeostasis, shaping the design in a new wave of therapeutically focused synthetic anion transporters.

EXPERIMENTAL PROCEDURES

Resource availability

Lead contact

Further information and requests for resources should be directed to and will be fulfilled by the lead contact, Philip Gale (philip.gale@uts.edu.au).

Materials availability

Full experimental procedures are provided in the supplemental information. Crystallographic data of **10** have been deposited in the Cambridge Crystallographic Data Centre (CCDC) under accession numbers CCDC: 2268417. The data can be obtained free of charge at https://www.ccdc.cam.ac.uk/structures/.

SUPPLEMENTAL INFORMATION

Supplemental information can be found online at .

ACKNOWLEDGMENTS

The authors acknowledge and pay respect to the Gadigal people of the Eora Nation, the traditional owners of the land on which we research, teach, and collaborate at The University of Technology Sydney and the University of Sydney. P. A. G. thanks The Australian Research Council (DP200100453) and The University of Technology Sydney for funding. E. J. N and M. E. G thank The Australian Research Council (CE200100012, DP210102148) for funding. W. G. R. gratefully acknowledges financial support through the Paulette Isabel Jones Career Award at the University of Sydney and the Faculty of Medicine and Health Shared Research Laboratories (University of Sydney) for the use of Guava flow cytometer. Figures 4, 5 and 6 were created in part with BioRender.com

AUTHOR CONTRIBUTIONS

Conceptualization W.G.R., E.J.N., and P.A.G. W.G.R. synthesized and characterized the compounds, performed the anion binding, transport, and spectroscopic data curation. B.A.H. and D.E.H. conducted the crystallography. W.G.R., M.E.G., and A.L. performed the fluorescence microscopy and cellular studies. W.G.R wrote the manuscript and all authors contributed to editing. E.J.N .and P.A.G supervised the project.

DECLARATION OF INTERESTS

The authors declare no competing interests.

REFERENCES

1. Ashcroft, F.M. (2001). Ion Channels and Disease (Academic Press).
2. EE Bittar, N.B. (1997). Principles of Medical Biology (JAI Press).
3. Gadsby, D.C. (2009). Ion channels versus ion pumps: the principal difference, in principle.

Nat. Rev. Mo.l Cell. Biol. 10, 344-352. 10.1038/nrm2668.
4. Hatta, S., Sakamoto, J., and Horio, Y. (2002). Ion channels and diseases. Med. Electron. Microsc. 35, 117-126. 10.1007/s007950200015
5. Li, H., Valkenier, H., Thorne, A.G., Dias, C.M., Cooper, J.A., Kieffer, M., Busschaert, N., Gale, P.A., Sheppard, D.N., and Davis, A.P. (2019). Anion carriers as potential treatments for cystic fibrosis: transport in cystic fibrosis cells, and additivity to channel-targeting drugs. Chem. Sci. 10, 9663-9672. 10.1039/c9sc04242c.
6. Ohkuma, S., Sato, T., Okamoto, M., Matsuya, H., Arai, K., Kataoka, T., Nagai, K., and Wasserman, H.H. (1998). Prodigiosins uncouple lysosomal vacuolar-type ATPase through promotion of H+/Cl- symport. Biochem J 334, 731-741. 10.1042/bj3340731.
7. Valkenier, H., Judd, L.W., Li, H., Hussain, S., Sheppard, D.N., and Davis, A.P. (2014). Preorganized bis-thioureas as powerful anion carriers: chloride transport by single molecules in large unilamellar vesicles. J. Am. Chem. Soc. 136, 12507-12512. 10.1021/ja507551z.
8. Wu, X., Small, J.R., Cataldo, A., Withecombe, A.M., Turner, P., and Gale, P.A. (2019). Voltage-Switchable HCl Transport Enabled by Lipid Headgroup-Transporter Interactions. Angew. Chem. Int. Ed. 58, 15142-15147. 10.1002/anie.201907466.
9. Davis, J.T., Gale, P.A., and Quesada, R. (2020). Advances in anion transport and supramolecular medicinal chemistry. Chem. Soc. Rev. 49, 6056-6086. 10.1039/c9cs00662a.
10. Park, S.H., Park, S.H., Howe, E.N.W., Hyun, J.Y., Chen, L.J., Hwang, I., Vargas-Zuniga, G., Busschaert, N., Gale, P.A., Sessler, J.L., and Shin, I. (2019). Determinants of Ion-Transporter Cancer Cell Death. Chem 5, 2079-2098. 10.1016/j.chempr.2019.05.001.
11. Busschaert, N., Park, S.H., Baek, K.H., Choi, Y.P., Park, J., Howe, E.N.W., Hiscock, J.R., Karagiannidis, L.E., Marques, I., Felix, V., et al. (2017). A synthetic ion transporter that disrupts autophagy and induces apoptosis by perturbing cellular chloride concentrations. Nat. Chem. 9, 667-675. 10.1038/nchem.2706.
12. Dard, L., Blanchard, W., Hubert, C., Lacombe, D., and Rossignol, R. (2020). Mitochondrial functions and rare diseases. Mol. Aspects. Med. 71, 100842. 10.1016/j.mam.2019.100842.
13. Schwarz, D.S., and Blower, M.D. (2016). The endoplasmic reticulum: structure, function and response to cellular signaling. Cell. Mol. Life Sci. 73, 79-94. 10.1007/s00018-015-2052-6.
14. Day, K.J., Staehelin, L.A., and Glick, B.S. (2013). A three-stage model of Golgi structure and function. Histochem. Cell Biol. 140, 239-249. 10.1007/s00418-013-1128-3.
15. J. M. Willard, F.R.M., and S. Lu. (2016). Lysosomes : Biology, Diseases, and Therapeutics (John Wiley & Sons).
16. O'Rourke, B. (2007). Mitochondrial ion channels. Annu. Rev. Physiol. 69, 19-49. 10.1146/annurev.physiol.69.031905.163804.
17. Duncan, R.R., Westwood, P.K., Boyd, A., and Ashley, R.H. (1997). Rat brain p64H1, expression of a new member of the p64 chloride channel protein family in endoplasmic reticulum. J. Biol. Chem. 272, 23880-23886. 10.1074/jbc.272.38.23880.
18. Maeda, Y., Ide, T., Koike, M., Uchiyama, Y., and Kinoshita, T. (2008). GPHR is a novel anion channel critical for acidification and functions of the Golgi apparatus. Nat. Cell. Biol. 10, 1135-1145. 10.1038/ncb1773.
19. Guo, L., Mao, Q., He, J., Liu, X., Piao, X., Luo, L.,

Hao, X., Yu, H., Song, Q., Xiao, B., et al. (2023). Disruption of ER ion homeostasis maintained by an ER anion channel CLCC1 contributes to ALS-like pathologies. Cell Res. 0, 1-19.

20. Banerjee, S., Veale, E.B., Phelan, C.M., Murphy, S.A., Tocci, G.M., Gillespie, L.J., Frimannsson, D.O., Kelly, J.M., and Gunnlaugsson, T. (2013). Recent advances in the development of 1,8-naphthalimide based DNA targeting binders, anticancer and fluorescent cellular imaging agents. Chem. Soc. Rev. 42, 1601-1618. 10.1039/c2cs35467e.
21. Geraghty, C., Wynne, C., and Elmes, R.B.P. (2021). 1,8-Naphthalimide based fluorescent sensors for enzymes. Coord. Chem. Rev. 437. 10.1016/j.ccr.2020.213713.
22. Amendola, V., Fabbrizzi, L., and Mosca, L. (2010). Anion recognition by hydrogen bonding: urea-based receptors. Chem. Soc. Rev. 39, 3889-3915. 10.1039/b822552b.
23. Berry, S.N., Soto-Cerrato, V., Howe, E.N.W., Clarke, H.J., Mistry, I., Tavassoli, A., Chang, Y.T., Perez-Tomas, R., and Gale, P.A. (2016). Fluorescent transmembrane anion transporters: shedding light on anionophoric activity in cells. Chem. Sci. 7, 5069-5077. 10.1039/c6sc01643j.
24. Lin, J., Yang, K., and New, E.J. (2021). Strategies for organelle targeting of fluorescent probes. Org. Biomol. Chem. 19, 9339-9357. 10.1039/d1ob01447a.
25. Handbook, T.M.P. (2010). 11 Edition (Life Technologies).
26. Munan, S., Ali, M., Yadav, R., Mapa, K., and Samanta, A. (2022). PET- and ICT-Based Ratiometric Probe: An Unusual Phenomenon of Morpholine-Conjugated Fluorophore for Mitochondrial pH Mapping during Mitophagy. Anal. Chem. 94, 11633-11642. 10.1021/acs.analchem.2c02177.
27. Qiu, K., Ke, L., Zhang, X., Liu, Y., Rees, T.W., Ji, L., Diao, J., and Chao, H. (2018). Tracking mitochondrial pH fluctuation during cell apoptosis with two-photon phosphorescent iridium(iii) complexes. Chem. Commun. 54, 2421-2424. 10.1039/c8cc00299a.
28. Huang, Y., Zhang, Y., Huo, F., Chao, J., and Yin, C. (2022). A dual-targeted organelles SO2 specific probe for bioimaging in related diseases and food analysis. Chem. Eng. J. 433. 10.1016/j.cej.2021.133750.
29. Fang, L., Trigiante, G., Crespo-Otero, R., Hawes, C.S., Philpott, M.P., Jones, C.R., and Watkinson, M. (2019). Endoplasmic reticulum targeting fluorescent probes to image mobile Zn(2). Chem. Sci. 10, 10881-10887. 10.1039/c9sc04300d.
30. Tang, Y., Xu, A., Ma, Y., Xu, G., Gao, S., and Lin, W. (2017). A turn-on endoplasmic reticulum-targeted two-photon fluorescent probe for hydrogen sulfide and bio-imaging applications in living cells, tissues, and zebrafish. Sci. Rep. 7, 12944. 10.1038/s41598-017-13325-z.
31. Xiao, H., Wu, C., Li, P., Gao, W., Zhang, W., Zhang, W., Tong, L., and Tang, B. (2017). Ratiometric photoacoustic imaging of endoplasmic reticulum polarity in injured liver tissues of diabetic mice. Chem. Sci. 8, 7025-7030. 10.1039/c7sc02330h.
32. Murphy, M.P., and Hartley, R.C. (2018). Mitochondria as a therapeutic target for common pathologies. Nat. Rev. Drug Discov. 17, 865-886. 10.1038/nrd.2018.174.
33. Zielonka, J., Joseph, J., Sikora, A., Hardy, M., Ouari, O., Vasquez-Vivar, J., Cheng, G., Lopez, M., and Kalyanaraman, B. (2017). Mitochondria-Targeted Triphenylphosphonium-Based Compounds: Syntheses, Mechanisms of Action, and Therapeutic and Diagnostic Applications. Chem. Rev. 117, 10043-10120.

10.1021/acs.chemrev.7b00042.
34. https://app.supramolecular.org.
35. Brynn Hibbert, D., and Thordarson, P. (2016). The death of the Job plot, transparency, open science and online tools, uncertainty estimation methods and other developments in supramolecular chemistry data analysis. Chem. Comm. 52, 12792-12805. 10.1039/c6cc03888c.
36. Barisic, D., Cindro, N., Vidovic, N., Bregovic, N., and Tomisic, V. (2021). Protonation and anion-binding properties of aromatic sulfonylurea derivatives. RSC Adv. 11, 23992-24000. 10.1039/d1ra04738h.
37. Jowett, L.A., and Gale, P.A. (2019). Supramolecular methods: the chloride/nitrate transmembrane exchange assay. Supramol. Chem. 31, 297-312. 10.1080/10610278.2019.1574017.
38. Behera, H., and Madhavan, N. (2017). Anion-Selective Cholesterol Decorated Macrocyclic Transmembrane Ion Carriers. J. Am. Chem. Soc. 139, 12919-12922. 10.1021/jacs.7b07479.
39. Mori, M., Sato, K., Ekimoto, T., Okumura, S., Ikeguchi, M., Tabata, K.V., Noji, H., and Kinbara, K. (2021). Imidazolinium-based Multiblock Amphiphile as Transmembrane Anion Transporter. Chem. Asian J. 16, 147-157. 10.1002/asia.202001106.
40. Chen, S., Zhang, S., Bao, C., Wang, C., Lin, Q., and Zhu, L. (2016). Oligo(aryl-triazole)s CHCl(-) interactions guide chloride efficient and selective transmembrane transport. Chem. Commun. 52, 13132-13135. 10.1039/c6cc07792g.
41. Yang, K., Boles, J.E., White, L.J., Hilton, K.L.F., Lai, H.Y., Long, Y., Hiscock, J.R., and Haynes, C.J.E. (2022). A water-soluble membrane transporter for biologically relevant cations. RSC Adv. 12, 27877-27880. 10.1039/d2ra05314d.
42. McNaughton, D.A., To, T.Y.T., Hawkins, B.A., Hibbs, D.E., and Gale, P.A. (2021). Delivering anion transporters to lipid bilayers in water. Org. Biomol. Chem. 19, 9624-9628. 10.1039/d1ob02041b.
43. Gilchrist, A.M., Wang, P., Carreira-Barral, I., Alonso-Carrillo, D., Wu, X., Quesada, R., and Gale, P.A. (2021). Supramolecular methods: the 8-hydroxypyrene-1,3,6-trisulfonic acid (HPTS) transport assay. Supramol. Chem. 33, 325-344. 10.1080/10610278.2021.1999956.
44. Spooner, M.J., and Gale, P.A. (2015). Anion transport across varying lipid membranes--the effect of lipophilicity. Chem. Commun. 51, 4883-4886. 10.1039/c5cc00823a.
45. Jowett, L.A., Howe, E.N.W., Soto-Cerrato, V., Van Rossom, W., Perez-Tomas, R., and Gale, P.A. (2017). Indole-based perenosins as highly potent HCl transporters and potential anti-cancer agents. Sci. Rep. 7, 9397. 10.1038/s41598-017-09645-9.
46. Singh, D., Rajput, D., and Kanvah, S. (2022). Fluorescent probes for targeting endoplasmic reticulum: design strategies and their applications. Chem. Commun. 58, 2413-2429. 10.1039/d1cc06944f.
47. Soto-Cerrato, V., Manuel-Manresa, P., Hernando, E., Calabuig-Farinas, S., Martinez-Romero, A., Fernandez-Duenas, V., Sahlholm, K., Knopfel, T., Garcia-Valverde, M., Rodilla, A.M., et al. (2015). Facilitated Anion Transport Induces Hyperpolarization of the Cell Membrane That Triggers Differentiation and Cell Death in Cancer Stem Cells. J. Am. Chem. Soc. 137, 15892-15898. 10.1021/jacs.5b09970.
48. Ko, S.K., Kim, S.K., Share, A., Lynch, V.M., Park, J., Namkung, W., Van Rossom, W., Busschaert, N., Gale, P.A., Sessler, J.L., and

Shin, I. (2014). Synthetic ion transporters can induce apoptosis by facilitating chloride anion transport into cells. Nat. Chem. 6, 885-892. 10.1038/nchem.2021.

49. Manuel-Manresa, P., Korrodi-Gregorio, L., Hernando, E., Villanueva, A., Martinez-Garcia, D., Rodilla, A.M., Ramos, R., Fardilha, M., Moya, J., Quesada, R., et al. (2017). Novel Indole-based Tambjamine-Analogues Induce Apoptotic Lung Cancer Cell Death through p38 Mitogen-Activated Protein Kinase Activation. Mol. Cancer Ther. 16, 1224-1235. 10.1158/1535-7163.MCT-16-0752.
50. Zimmermann, M., and Meyer, N. (2011). Mammalian Cell Viability. Methods in Molecular Biology. 10.1007/978-1-61779-108-6.
51. Tabas, I., and Ron, D. (2011). Integrating the mechanisms of apoptosis induced by endoplasmic reticulum stress. Nat. Cell Biol. 13, 184-190. 10.1038/ncb0311-184.
52. Verfaillie, T., Garg, A.D., and Agostinis, P. (2013). Targeting ER stress induced apoptosis and inflammation in cancer. Cancer Lett. 332, 249-264. 10.1016/j.canlet.2010.07.016.
53. Puthalakath, H., O'Reilly, L.A., Gunn, P., Lee, L., Kelly, P.N., Huntington, N.D., Hughes, P.D., Michalak, E.M., McKimm-Breschkin, J., Motoyama, N., et al. (2007). ER stress triggers apoptosis by activating BH3-only protein Bim. Cell 129, 1337-1349. 10.1016/j.cell.2007.04.027.
54. Kannan, K., and Jain, S.K. (2000). Oxidative stress and apoptosis. Pathophysiology 7, 153-163. 10.1016/s0928-4680(00)00053-5.
55. Chen, Y., McMillan-Ward, E., Kong, J., Israels, S.J., and Gibson, S.B. (2008). Oxidative stress induces autophagic cell death independent of apoptosis in transformed and cancer cells. Cell Death Differ. 15, 171-182.